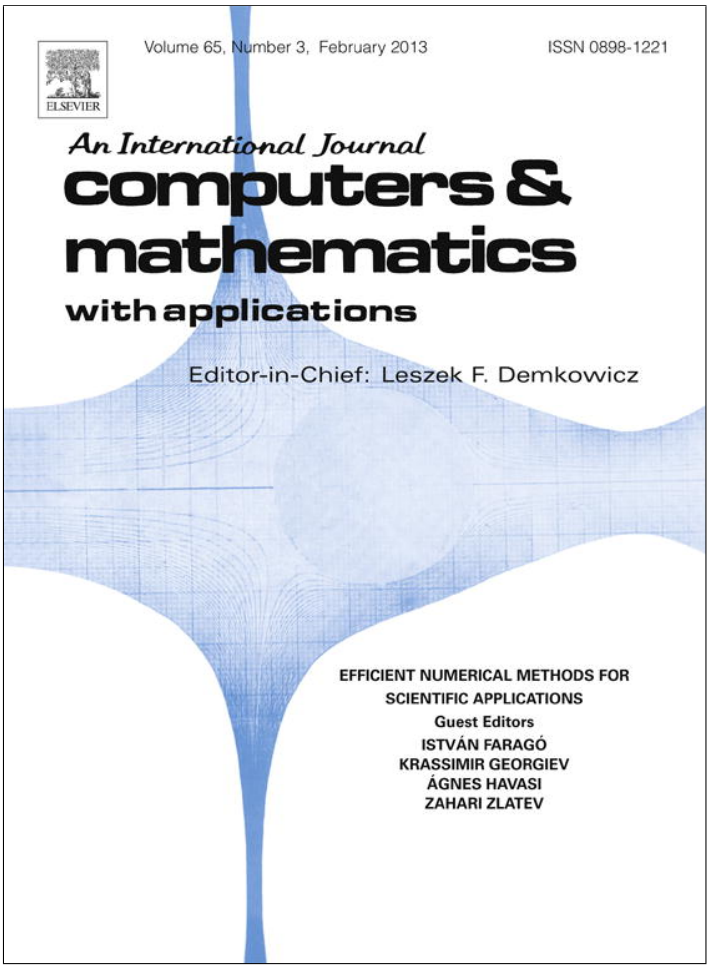

Computers and Mathematics with Applications 65 (2013) 520–527

Contents lists available at SciVerse ScienceDirect

Computers and Mathematics with Applications

journal homepage: www.elsevier.com/locate/camwa

A variance-reduced electrothermal Monte Carlo method for semiconductor device simulation

Orazio Muscato [a], Vincenza Di Stefano [a], Wolfgang Wagner [b,*]

[a] Dipartimento di Matematica e Informatica, Viale Andrea Doria 6 - 95125 Catania, Italy

[b] Weierstrass Institute for Applied Analysis and Stochastics, Mohrenstrasse 39 - 10117 Berlin, Germany

ARTICLE INFO

Keywords:
Semiconductor devices
Monte Carlo simulation
Electrothermal modelling

ABSTRACT

This paper is concerned with electron transport and heat generation in semiconductor devices. An improved version of the electrothermal Monte Carlo method is presented. This modification has better approximation properties due to reduced statistical fluctuations. The corresponding transport equations are provided and results of numerical experiments are presented.

1. Introduction

The Monte Carlo method is one of the common techniques for modelling electron transport in semiconductors [1–3]. It is based on Boltzmann transport equations, which describe the time evolution of the distribution of electrons with respect to position and wave-vector. One of the main advantages of the Monte Carlo method is its ability to include a large range of physical effects. The continued miniaturization of semiconductor devices has resulted in new challenges related to the modelling of heat generation.

Recently an electrothermal Monte Carlo method has been developed [4–7]. The method couples a stochastic algorithm for the Boltzmann transport equation with a steady-state solution of the heat diffusion equation. The lattice heating rate is calculated by accounting for the exchange of phonons between the electrons and the lattice. This net phonon emission method was applied in [8] without including heat diffusion effects. A survey on heat generation and transport in transistors was given in [9].

The purpose of the paper is to study the electrothermal Monte Carlo method and to present a modification with reduced statistical fluctuations. The paper is organized as follows. Details of the mathematical model are provided in Section 2. A variance-reduced electrothermal Monte Carlo method is proposed in Section 3. Results of numerical experiments are presented in Section 4. Comments and conclusions are given in Section 5.

2. Kinetic equations for electrons

In a semiclassical approximation, the kinetic description of electron transport is given by the equation

$$\left[\frac{\partial}{\partial t} + v(k)\cdot\nabla_x - \frac{q}{\hbar}E(t,x)\cdot\nabla_k\right] f(t,x,k) = (Qf)(t,x,k), \tag{1}$$

* Corresponding author.
E-mail addresses: muscato@dmi.unict.it (O. Muscato), vdistefano@dmi.unict.it (V. Di Stefano), wagner@wias-berlin.de (W. Wagner).

0898-1221/$ – see front matter © 2013 Published by Elsevier Ltd
doi:10.1016/j.camwa.2012.03.100

which determines the time evolution of the distribution $f(t, x, k)$ of electrons with respect to position x and wave-vector k. The electric field E depends on the electron distribution function f. It is defined as

$$E(t, x) = -\nabla_x \Phi(t, x), \tag{2}$$

where the electric potential Φ satisfies the Poisson equation

$$\epsilon \, \Delta_x \Phi(t, x) = q \, [n(t, x) - n_D(x)] \, . \tag{3}$$

The function

$$n(t, x) = \int_{\mathbb{R}^3} f(t, x, k) \, dk \tag{4}$$

is the electron density and n_D denotes the donor density. Moreover, q is the absolute value of the electron charge, ϵ is the permittivity, $\hbar$ denotes Planck's constant divided by 2π and $\mathbb{R}^3$ is the Euclidean space. Boundary conditions to (3) take into account an external field. Boundary conditions to (1) are more complicated. In the spatially one-dimensional case we assume periodic boundaries.

We consider analytic conduction bands in the quasi-parabolic approximation, where the kinetic energy $\varepsilon(k)$ of an electron satisfies the relation

$$\varepsilon(k) \, [1 + \alpha \varepsilon(k)] = \frac{\hbar^2 \, |k|^2}{2m^\star}, \quad k \in \mathbb{R}^3. \tag{5}$$

Here α denotes the non-parabolicity factor (the case $\alpha = 0$ is called parabolic) and $m^\star$ is the effective electron mass. If $\alpha > 0$, then (5) implies

$$\varepsilon(k) = \frac{\sqrt{1 + \frac{2\alpha \, \hbar^2 \, |k|^2}{m^*}} - 1}{2\alpha}. \tag{6}$$

The electron group velocity $v(k)$ takes the form

$$v(k) = \frac{1}{\hbar} \, \nabla_k \, \varepsilon(k) = \frac{\hbar k}{m^\star [1 + 2\alpha \varepsilon(k)]}. \tag{7}$$

The quasi-parabolic band approximation provides a good description of electron transport at energies up to 1 eV, where impact ionization does not play a significant role.

The scattering collision operator has the form

$$(Q \, f)(t, x, k) = \int_{\mathbb{R}^3} S(k', k) \, f(t, x, k') \, dk' - f(t, x, k) \int_{\mathbb{R}^3} S(k, k') \, dk'. \tag{8}$$

The main scattering mechanisms in silicon, at room temperature, are due to electron–phonon interactions (acoustic and optical). The transition rate from a state k to a state k' is determined by the function (cf. [1, Section III.D.1])

$$S(k, k') = S_{\text{ac}}(k, k') + S_{\text{opt}}(k, k'), \tag{9}$$

where

$$S_{\text{ac}}(k, k') = K_0 \, \delta(\varepsilon(k') - \varepsilon(k)) \tag{10}$$

and

$$S_{\text{opt}}(k, k') = \sum_{i=1}^{6} K_i \Big[\delta(\varepsilon(k') - \varepsilon(k) + \hbar\omega_i) \, (g_i + 1) + \delta(\varepsilon(k') - \varepsilon(k) - \hbar\omega_i) \, g_i \Big]. \tag{11}$$

The coefficients in (10), (11) are

$$K_0 = \frac{k_B \, T_L \, \Xi_d^2}{4\pi^2 \hbar \, \rho \, v_s^2} \tag{12}$$

and

$$K_i = \frac{(D_t K)_i^2 Z_i}{8\pi^2 \rho \, \omega_i}, \quad i = 1, \ldots, 6, \tag{13}$$

where k_B denotes Boltzmann's constant, T_L is the lattice temperature and further parameters are given in Tables 1, 2. Finally, the phonon occupation numbers in (11) are

$$g_i = \frac{1}{\exp(\hbar\omega_i / k_B T_L) - 1}. \tag{14}$$

We refer to [2, Section 2.2.5] for further details of the modelling.

Table 1
Silicon parameters.

m_e	Electron rest mass	9.1095×10^{-28} g
$m^\star$	Effective mass	$0.3216\, m_e$
ρ	Mass density	2.33 g/cm^3
v_s	Longitudinal sound speed	9.18×10^5 cm/s
Ξ_d	Acoustic phonon deformation potential	9 eV
α	Non-parabolicity factor	0.5 eV^{-1}

Table 2
Coupling constants for optical phonon scattering.

i	Scattering (branch)	$\hbar\omega_i$ (meV)	$(D_t K)_i$ (eV Å^{-1})	Z_i
1	g-1 (TA)	12	0.5	1
2	g-2 (LA)	18.5	0.8	1
3	g-3 (LO)	61.2	11	1
4	f-1 (TA)	19.0	0.3	4
5	f-2 (LA)	47.4	2.0	4
6	f-3 (TO)	59.0	2.0	4

3. The Monte Carlo algorithm

The Monte Carlo approach is based on a stochastic particle system of the form

$$(x_l(t), k_l(t)) \quad l = 1, \ldots, N \quad t \geq 0. \tag{15}$$

A time step Δt is used to decouple the transport equation (1) and the Poisson equation (3). That is, each particle moves with its velocity (7), performs scatterings according to the transition rate function (9) and is accelerated according to a fixed electric field. After Δt, the density (4) is measured and the field is re-calculated according to (2), (3).

The system (15) provides a numerical algorithm for Eq. (1) in the sense that linear functionals of the solution f are approximated by averages over the particle system, that is

$$\int_{\Delta x}\int_{\mathbb{R}^3} \varphi(k) f(t, x, k)\, dk\, dx \sim \frac{1}{N} \sum_{l:\, x_l(t)\in\Delta x} \varphi(k_l(t)), \tag{16}$$

for some spatial cell Δx and appropriate test functions φ. Convergence with respect to the numerical parameters ($N \to \infty$ and $\Delta t \to 0$) has been studied in [10].

The steady state is approximated by a time averaging procedure, that is

$$\int_{\Delta x}\int_{\mathbb{R}^3} \varphi(k) f(\infty, x, k)\, dk\, dx \sim \frac{1}{N_{\text{obs}}} \sum_{j=1}^{N_{\text{obs}}} \Phi(t_j, \Delta x), \tag{17}$$

where $\Phi(t, \Delta x)$ is a notation for the right-hand side of (16) and t_j, $j = 1, \ldots, N_{\text{obs}}$, are observation points (far enough from $t = 0$). Properties of the steady state distribution have been studied in [11].

3.1. Scattering mechanisms

The operator (8) has a probabilistic interpretation in terms of random jump processes, where the jumps are determined by various scattering mechanisms. The transition rate function (10) corresponds to acoustic (elastic) scattering, which means that the energy of the electron is preserved and it just gets a new orientation. The transition rate function (11) corresponds to optical (inelastic) scattering, which means that the electron either looses energy (interpreted as emission of a phonon) or gains energy (interpreted as absorption of a phonon). The quantities $\hbar\omega_i$ in (11) are phonon energies (cf. Table 2). Emission of a phonon is only possible if $\varepsilon(k) > \hbar\omega_i$, otherwise the electron does not have enough energy.

The relative frequencies of various scattering events are determined by the corresponding rates. The acoustic scattering rate takes the form

$$\int_{\mathbb{R}^3} S_{\text{ac}}(k, k')\, dk' = \lambda_{\text{ac}}(\varepsilon(k)), \tag{18}$$

where [1, Eq. (3.54)]

$$\lambda_{\text{ac}}(\varepsilon) = T_L \frac{2^{\frac{1}{2}} m^{*\frac{3}{2}} k_B \Xi_d^2}{\pi\, \hbar^4\, \rho v_s^2} (1 + 2\alpha\varepsilon) \sqrt{\varepsilon(1 + \alpha\varepsilon)}. \tag{19}$$

The optical scattering rate takes the form

$$\int_{\mathbb{R}^3} S_{\text{opt}}(k, k')\, dk' = \sum_{i=1}^{6} \left[\lambda_i^+(\varepsilon(k)) + \lambda_i^-(\varepsilon(k)) \right], \tag{20}$$

where [1, Eq. (3.73)]

$$\lambda_i^+(\varepsilon) = (g_i(T_L) + 1) \frac{(D_t K)_i^2 m^{*\frac{3}{2}} Z_i}{2^{\frac{1}{2}} \pi\, \hbar^3\, \rho \omega_i} \sqrt{(\varepsilon - \hbar\omega_i)[1 + \alpha(\varepsilon - \hbar\omega_i)]}[1 + 2\alpha(\varepsilon - \hbar\omega_i)], \tag{21}$$

if $\varepsilon > \hbar\omega_i$ (otherwise, $\lambda_i^+(\varepsilon) = 0$), and

$$\lambda_i^-(\varepsilon) = g_i(T_L) \frac{(D_t K)_i^2 m^{*\frac{3}{2}} Z_i}{2^{\frac{1}{2}} \pi\, \hbar^3\, \rho \omega_i} \sqrt{(\varepsilon + \hbar\omega_i)[1 + \alpha(\varepsilon + \hbar\omega_i)]}[1 + 2\alpha(\varepsilon + \hbar\omega_i)]. \tag{22}$$

The signs "+" and "−" indicate emission and absorption of a phonon, and the dependence of the expressions (14) on the lattice temperature is emphasized.

3.2. The electrothermal Monte Carlo method

The main steps of the algorithm are the following:

1. The standard isothermal Monte Carlo algorithm is run until the steady-state is reached.
2. Various electronic parameters are sampled to generate the results from this iteration. In particular, the sum over all phonon emission minus phonon absorption events per unit time is calculated, i.e. [9, p. 1590]

$$\langle H^C \rangle(x) = \frac{n}{N_p\, t_{\text{sim}}} \sum_{i=1}^{6} \hbar\omega_j \left[C_i^+ - C_i^- \right], \tag{23}$$

where n is the electron density, N_p is the number of particles in the x-cell, t_{sim} is total simulation time after the steady-state has been reached, and C_i^+, C_i^- are the total numbers of i-th phonons emitted and absorbed. The quantity (23) is used as an approximation to the rate of heat generation at position x,

$$g(x) = \langle H^C \rangle(x). \tag{24}$$

3. The spatially varying lattice temperature distribution $T_L(x)$ is obtained by solving the steady-state heat diffusion equation [6, p. 1769]

$$\nabla_x \cdot (\kappa\, \nabla_x T_L(x)) + g(x) = 0, \tag{25}$$

where κ is the thermal conductivity (in Silicon at room temperature 150 W/K m) and $g(x)$ is the rate of heat generation at position x.
4. In the next iteration the Monte Carlo algorithm is rerun with the new update lattice temperature distribution $T_L(x)$. Note that the scattering rates (19), (21) and (22) depend on the lattice temperature.
5. This iterative procedure is performed until the terminal currents converge to the electrothermal steady-state values.

3.3. The variance-reduced electrothermal Monte Carlo method

We modify step 2 of the algorithm described in Section 3.2. The heat generation rate is approximated using the individual optical scattering rates (21), (22). Instead of (24), we use

$$g(x) = \langle H \rangle(x), \tag{26}$$

where (cf. (15))

$$\langle H \rangle(x) = \frac{1}{N_{\text{obs}}} \sum_{j=1}^{N_{\text{obs}}} \left[\frac{n}{N_p} \sum_{l=1}^{N_p} G(\varepsilon(k_l(t_j))) \right] \tag{27}$$

and

$$G(\varepsilon) = \sum_{i=1}^{6} \hbar\omega_i \left[\lambda_i^+(\varepsilon) - \lambda_i^-(\varepsilon) \right]. \tag{28}$$

Here n is the electron density, N_p is the number of particles in the x-cell and N_{obs} is the total number of observation times t_j.

The introduction of the function (28) reduces the evaluation of heat generation to the usual calculation of functionals, in analogy with mean velocity or mean energy. Moreover, the functional (27) indicates which system of kinetic equations is actually solved by the electrothermal Monte Carlo algorithm. Namely, the steady state heat diffusion equation (25) is coupled to the steady state version of the Boltzmann transport equation (1) via

$$g(x) = \int_{\mathbb{R}^3} G(\varepsilon(k))\, f(\infty, x, k)\, dk. \tag{29}$$

In order to illustrate the connection between the expressions (23) and (27), we introduce the quantities

$$h^C(s,t) = \sum_{i=1}^{6} \hbar\omega_i \left[C_i^+(s,t) - C_i^-(s,t)\right], \tag{30}$$

where $C_i^+(s,t)$, $C_i^-(s,t)$ are the numbers of i-th phonons emitted and absorbed on the time interval $[s,t]$. Expression (23) takes the form

$$\begin{aligned}\langle H^C\rangle(x) &= \frac{n}{N_p\, t_{\mathrm{sim}}}\, h^C(t_0, t_0 + t_{\mathrm{sim}}) = \frac{n\, N_{\mathrm{obs}}}{N_p\, t_{\mathrm{sim}}} \frac{1}{N_{\mathrm{obs}}} \sum_{j=1}^{N_{\mathrm{obs}}} h^C(t_{j-1}, t_j) \\ &= \frac{1}{N_{\mathrm{obs}}} \sum_{j=1}^{N_{\mathrm{obs}}} \frac{n}{N_p} \frac{h^C(t_{j-1}, t_j)}{\Delta t_{\mathrm{obs}}},\end{aligned} \tag{31}$$

where t_0 denotes the starting point for time averaging and Δt_{obs} is the observation time step. The connection between the expressions (31) and (27) is based on the fact that the average number of jumps on some time interval is approximately given by the product of the jump rate and the length of the interval.

It turns out that the variance of the estimator (23) is always bigger than the variance of the estimator (27). This is a consequence of the formula

$$\mathbb{V}(\xi) = \mathbb{V}(\mathbb{E}(\xi|\eta)) + \mathbb{E}\,\mathbb{V}(\xi|\eta), \tag{32}$$

which says that the variance of any scalar random variable ξ can be represented as the sum of the variance of the conditional expectation and the expectation of the conditional variance. The conditional expectation can be taken with respect to an arbitrary random variable η with a rather general state space (e.g., a random vector). Formula (32), which is sometimes called "law of total variance", is a direct consequence of the corresponding definitions,

$$\begin{aligned}&\mathbb{V}(\xi) = \mathbb{E}(\xi - \mathbb{E}\xi)^2 = \mathbb{E}\xi^2 - (\mathbb{E}\xi)^2 \\ &\mathbb{V}(\mathbb{E}(\xi|\eta)) = \mathbb{E}(\mathbb{E}(\xi|\eta))^2 - (\mathbb{E}\,\mathbb{E}(\xi|\eta))^2 = \mathbb{E}(\mathbb{E}(\xi|\eta))^2 - (\mathbb{E}\xi)^2 \\ &\mathbb{V}(\xi|\eta) = \mathbb{E}([\xi - \mathbb{E}(\xi|\eta)]^2|\eta) = \mathbb{E}(\xi^2|\eta) - (\mathbb{E}(\xi|\eta))^2.\end{aligned}$$

In the present situation, η is the whole particle system (15), while ξ is the estimator (23). According to (31), the estimator (27) has the form $\mathbb{E}(\xi|\eta)$.

4. Numerical experiments

In this section we illustrate the two different ways (23) and (27) of evaluating the heat generation rate. First the spatially homogeneous situation (bulk case) is considered. Then a spatially one-dimensional test case (diode) is studied. In both cases we use the parabolic band approximation (cf. (5)) and periodic boundary conditions. The algorithm described in Section 3.2 is applied with 4 iterations.

Confidence intervals are calculated as

$$\frac{1}{N_r}\sum_{\alpha=1}^{N_r} \xi_\alpha \pm 3\sqrt{\frac{1}{N_r}\left(\frac{1}{N_r}\sum_{\alpha=1}^{N_r}\xi_\alpha^2 - \left[\frac{1}{N_r}\sum_{\alpha=1}^{N_r}\xi_\alpha\right]^2\right)}, \tag{33}$$

where ξ_α, $\alpha = 1, \ldots, N_r$, denote the values of some quantity ξ obtained with independent runs (repetitions). In our situation, we have $\xi = \langle H\rangle$ and $\xi = \langle H^C\rangle$. The discretization parameters Δt and Δx are chosen in such a way that the corresponding systematic error is smaller than the bounds for the statistical error provided by confidence intervals.

4.1. Bulk case

Here the number of particles is $N = 11\,000$ and the number of repetitions is $N_r = 10$.

Table 3
The heat generation rate calculated via (23) and (27), with $T_L = 300$ K and various electric fields.

Field (V/cm)	$\langle H \rangle$ (10^{11} meV/s)	$\langle H^C \rangle$ (10^{11} meV/s)
0	-0.12 ± 0.26	-0.04 ± 0.47
10	-0.51 ± 0.51	-0.88 ± 0.85
100	-0.46 ± 0.36	-0.23 ± 0.75
1*k*	7.7 ± 0.3	7.9 ± 0.8
10*k*	544.1 ± 0.6	543.7 ± 1.3
100*k*	$10\,875 \pm 3$	$10\,874 \pm 5$

Table 4
The heat generation rate calculated via (23) and (27), with $T_L = 77$ K and various electric fields.

Field (V/cm)	$\langle H \rangle$ (10^{11} meV/s)	$\langle H^C \rangle$ (10^{11} meV/s)
0	-0.001 ± 0.018	-0.001 ± 0.044
10	0.746 ± 0.014	0.737 ± 0.046
100	0.752 ± 0.015	0.750 ± 0.037
1*k*	43.0 ± 0.12	42.9 ± 0.23
10*k*	1083 ± 0.3	1083 ± 0.7
100*k*	$21\,652 \pm 1.6$	$21\,653 \pm 2.5$

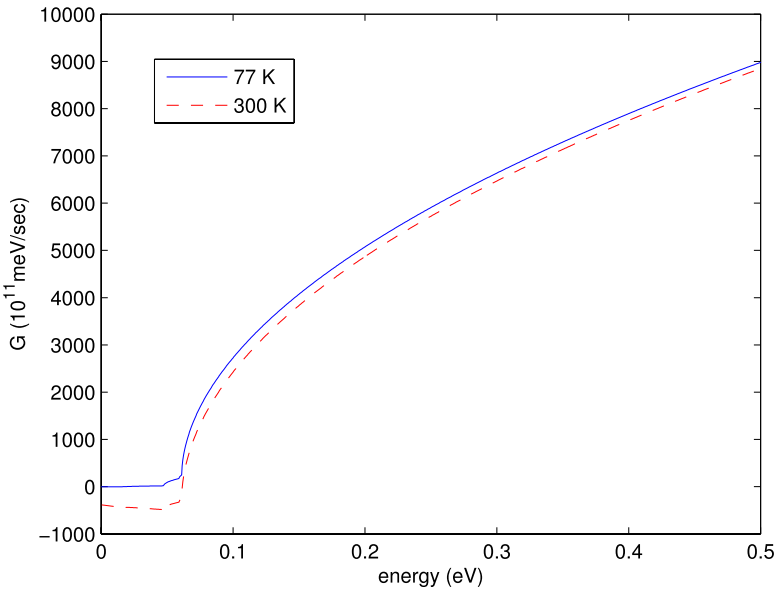

Fig. 1. Function (28) with $T_L = 300$ K and $T_L = 77$ K.

Results for the lattice temperature $T_L = 300$ K and various electric fields are shown in Table 3. The statistical error bounds (cf. (33)) are about two times smaller for the estimator (27) compared to those for the estimator (23). Moreover, some "cooling effect" (negative heat production) is observed for certain electric fields. In order to check this more precisely for the field 100 V/cm, the number of repetitions has been increased to $N_r = 40$. The corresponding values are

$$\begin{aligned} \langle H \rangle &= -0.49 \pm 0.16\,(10^{11}\ \text{meV/s}), \\ \langle H^C \rangle &= -0.57 \pm 0.38\,(10^{11}\ \text{meV/s}). \end{aligned} \tag{34}$$

Analogous results for the lattice temperature $T_L = 77$ K are shown in Table 4. The relationship between the statistical error bounds for both estimators is roughly the same, but no cooling is observed. The different behaviour dependent on the temperature is formally explained by the corresponding graphs of the function (28) provided in Fig. 1.

4.2. Diode

We consider a silicon $n^+ - n - n^+$ diode, which consists of two highly doped regions n^+ (called cathode and anode) connected by a less doped region n (called channel). The n^+ regions are 100 nm-long and doped to a density $N_D = 10^{19}$ cm^{-3}, while the channel is 100 nm-long and doped to a density $N_D = 10^{16}$ cm^{-3}. The applied bias is $V_b = 1.2$ V.

Here the total number of particles is $N = 201\,000$ and the number of repetitions is $N_r = 10$.

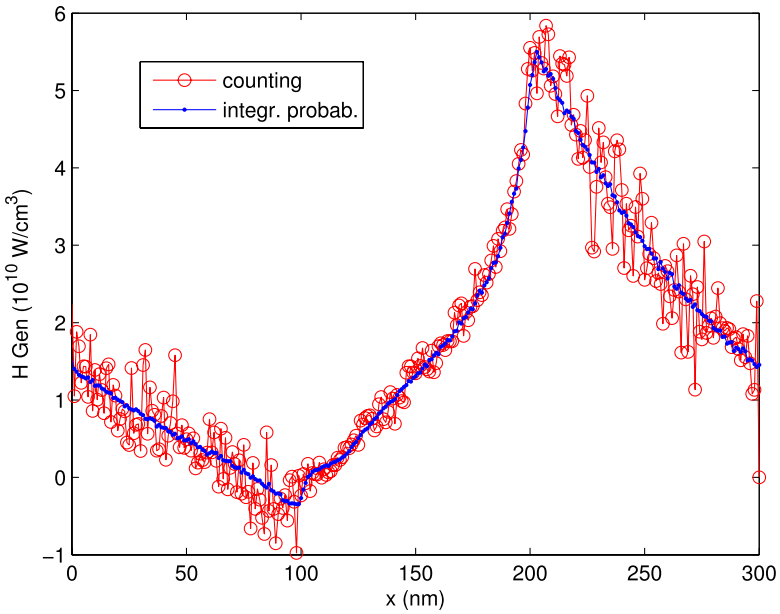

Fig. 2. Heat generation rate versus position in the diode, evaluated by means of the counting estimator (23) and the integrated probability estimator (27).

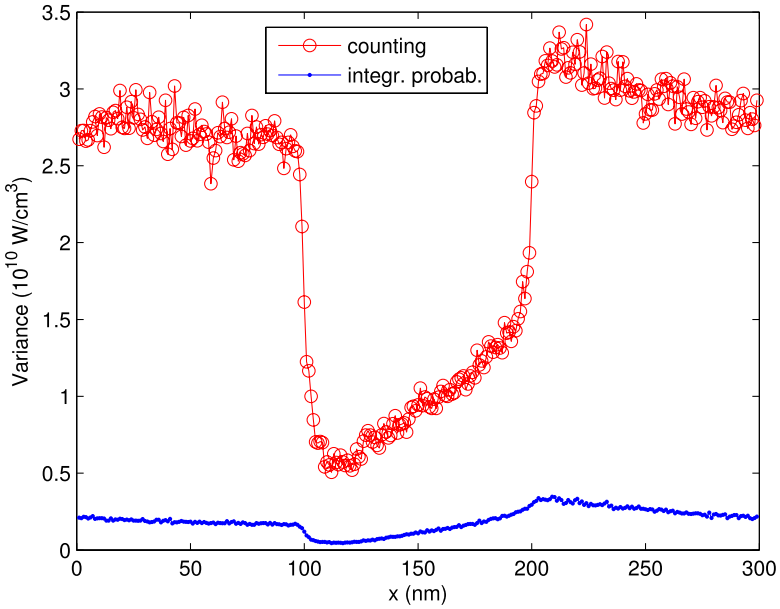

Fig. 3. Variances of the counting estimator (23) and the integrated probability estimator (27) versus position in the diode.

The results are shown in Fig. 2. The integrated probability estimator (27) has significantly lower fluctuations compared to the counting estimator (23). The absolute values of the variances are displayed in Fig. 3. At the left contact a "cooling effect" (negative heat production) is observed, while at the right contact there is a peak in the heat production.

5. Comments

A comparison between Monte Carlo and hydrodynamic simulations of heat generation and transport has been performed in [12]. This study illustrates the limitations of the hydrodynamic approach. An extension of the Monte Carlo algorithm for the treatment of the coupled system of kinetic equations for electrons and phonons has been used in [13,14]. The main drawback of this approach is the huge computational effort. The electrothermal Monte Carlo algorithm provides a rather efficient tool for studying heat generation and transport.

The modification proposed in this paper always leads to some variance reduction, which may be quite significant as illustrated in Section 4.2. In addition to this practically important effect, there are some other advantages of the new method. The estimator based on the function (28) reduces the evaluation of heat generation to the usual calculation of functionals, in analogy with mean velocity or mean energy. Moreover, it indicates that the electrothermal Monte Carlo algorithm solves the steady state Boltzmann transport equation coupled with a steady state heat diffusion equation.

The possible occurrence of negative heat production has been observed as a side effect of the numerical experiments illustrating the variance reduction. We do not have any convincing physical explanation for the bulk case. However, in the case of the diode, this observation might be related to the Peltier effect, which occurs at the junction of two different materials, where heat may be either generated or absorbed.

References

[1] C. Jacoboni, L. Reggiani, The Monte Carlo method for the solution of charge transport in semiconductors with applications to covalent materials, Rev. Modern Phys. 55 (3) (1983) 645–705.
[2] C. Jacoboni, P. Lugli, The Monte Carlo Method for Semiconductor Device Simulation, Springer, New York, 1989.
[3] M.V. Fischetti, S.E. Laux, P.M. Solomon, A. Kumar, Thirty years of Monte Carlo simulations of electronic transport in semiconductors: their relevance to science and mainstream VLSI technology, J. Comput. Electron. 3 (2004) 287–293.
[4] N.J. Pilgrim, W. Batty, R.W. Kelsall, Thermally self-consistent Monte Carlo device simulation, J. Comput. Electron. 1 (2002) 263–266.
[5] N.J. Pilgrim, W. Batty, R.W. Kelsall, Electrothermal Monte Carlo simulations of InGaAs/AlGaAs HEMTs, J. Comput. Electron. 2 (2003) 207–211.
[6] T. Sadi, R. Kelsall, N. Pilgrim, Simulation of electron transport in InGaAs/AlGaAs HEMTs using an electrothermal Monte Carlo method, IEEE Trans. Electron Devices 53 (8) (2006) 1768–1774.
[7] K. Raleva, D. Vasileska, S.M. Goodnick, M. Nedjalkov, Modeling thermal effects in nano-devices, IEEE Trans. Electron Devices 56 (6) (2008) 1306–1316.
[8] C. Moglestue, F.A. Buot, W.T. Anderson, Ensemble Monte Carlo particle investigation of hot electron induced source-drain burnout characteristics of GaAs field-effect transistors, J. Appl. Phys. 78 (4) (1995) 2343–2348.
[9] E. Pop, S. Sinha, K. Goodson, Heat generation and transport in nanometer scale transistors, Proc. IEEE 94 (8) (2006) 1587–1601.
[10] O. Muscato, W. Wagner, V. Di Stefano, Numerical study of the systematic error in Monte Carlo schemes for semiconductors, ESAIM: M2AN Math. Model. Numer. Anal. 44 (5) (2010) 1049–1068.
[11] O. Muscato, W. Wagner, V. Di Stefano, Properties of the steady state distribution of electrons in semiconductors, Kinet. Relat. Models 4 (3) (2011) 809–829.
[12] O. Muscato, V. Di Stefano, Heat generation and transport in nanoscale semiconductor devices via Monte Carlo and hydrodynamic simulations, COMPEL 30 (2) (2011) 519–537.
[13] J.A. Rowlette, K.E. Goodson, Fully coupled nonequilibrium electron–phonon transport in nanometer-scale silicon fets, IEEE Trans. Electron Devices 55 (1) (2008) 220–232.
[14] Z. Aksamija, U. Ravaioli, Anharmonic decay of non-equilibrium intervalley phonons in silicon, J. Phys. Conf. Ser. 193 (2009) 012033.